



**HAL**  
open science

## Shielding effectiveness of concrete reinforced with steel fibers: influence of fiber length and aspect ratio

Antoine Martin, Sébastien Brisard, Karam Sab, Salwa Ben Mbarek, Jean-Paul Caron-Fellens

► **To cite this version:**

Antoine Martin, Sébastien Brisard, Karam Sab, Salwa Ben Mbarek, Jean-Paul Caron-Fellens. Shielding effectiveness of concrete reinforced with steel fibers: influence of fiber length and aspect ratio. 2023. hal-04296863

**HAL Id: hal-04296863**

**<https://hal.science/hal-04296863>**

Preprint submitted on 20 Nov 2023

**HAL** is a multi-disciplinary open access archive for the deposit and dissemination of scientific research documents, whether they are published or not. The documents may come from teaching and research institutions in France or abroad, or from public or private research centers.

L'archive ouverte pluridisciplinaire **HAL**, est destinée au dépôt et à la diffusion de documents scientifiques de niveau recherche, publiés ou non, émanant des établissements d'enseignement et de recherche français ou étrangers, des laboratoires publics ou privés.

# Shielding effectiveness of concrete reinforced with steel fibers: influence of fiber length and aspect ratio

Antoine Martin<sup>a,b,\*</sup>, Sébastien Brisard<sup>a</sup>, Karam Sab<sup>a</sup>, Salwa Ben Mbarek<sup>c</sup>, Jean-Paul Caron-Fellens<sup>c</sup>

<sup>a</sup>Univ Gustave Eiffel, Ecole des Ponts, CNRS, Navier F-77454 Marne-la-Vallée, France

<sup>b</sup>Spie batignolles génie civil, 30 avenue du Général Gallieni, CS 10192, 92023 Nanterre CEDEX, France

<sup>c</sup>EuroMC, 2 avenue de Stalingrad, 93240 Stains, France

---

## Abstract

We present an experimental assessment of the electromagnetic shielding effectiveness of fiber-reinforced concrete slabs. The following parameters are varied: fiber volume content, fiber length and fiber aspect ratio, and the influence of each one can be observed. The measurements are compared to theoretical predictions by the Maxwell Garnett formula. This formula is known to apply only to low frequencies (quasi-static assumption). Based on our experiments, we propose a formula that defines the validity range of the underlying quasi-static assumption. Finally, we assess over a six month period how the evolution of the concrete matrix affects the shielding effectiveness of the fiber-reinforced concrete slab.

**Keywords:** Fiber-reinforced concrete, Shielding effectiveness, Aspect ratio, Homogenization, Quasi-static assumption

---

## 1. Introduction

Electromagnetic shielding is often required for buildings that host sensitive electronic facilities (intelligence headquarters, military or medical facilities, data centers, etc.). It is traditionally provided by Faraday cages; however, such devices are costly and their installation is difficult, requiring a fair amount of expertise.

Fiber-reinforced concrete (FRC) exhibits a good attenuation in the high-frequency range (Guan et al., 2006; Chung, 2000; Wen and Chung, 2004). Observing that wire meshes provide excellent attenuation at low-frequencies (Quintana et al., 2018; Yuan et al., 2021; Lee et al., 2021; Krause et al., 2012; Nguyen et al., 2017), two french companies, namely: *Spie batignolles génie civil* and *EuroMC* have recently patented GreyShield<sup>®</sup> (Caron-Fellens and Mardiguian, 2017). It provides electromagnetic shielding through the combination of FRC walls and wire meshes that are placed on the external surface.

Many researches focused on finding best combination for obtaining a good shielding effectiveness (SE).

Different kinds of cement-based shielding are thus obtained: with or without metallic grid (Yuan et al., 2021; Lee et al., 2021; Yuan et al., 2022), fibers or powders (Guan et al., 2006; Cao and Chung, 2003); effect of re-bars is analyzed (Yuan et al., 2021); and alternatives to steel additives are tested: carbon (Chung, 2000, 2001; Jung et al., 2020), taconite (Krause et al., 2012; Nguyen et al., 2017), ferrite (Stefaniuk et al., 2022).

Fibers, with their high aspect ratio, are interesting for different reasons. First, some authors explain that the percolation threshold is reached for a lower volume fraction with high aspect ratios inclusions (Yuan et al., 2021). It means that even though matrix is non conductive, the fibrous medium can become conductive, because of the fiber network. However, for shielding applications, for which frequencies are usually higher than the kiloHertz, concrete is conductive and there is, theoretically, no need to reach the percolation threshold. Second, because of their shape, metallic fibers embedded in a conductive matrix enhance the conductivity better than metallic powder would do for the same volume fraction. Actually, for low volume fractions, the effect of aspect ratio can be quantified by models (Solgaard et al., 2014). However, these formulas are not commonly used for estimating the shielding effectiveness in frequency regime.

---

\*Corresponding author:

Email address: antoine.martin@spiebatignolles.fr  
(Antoine Martin)

Actually, effect of aspect ratio, concentration but also fiber length, have not been clearly asserted on FRC: most of the time, measurements were carried out on specimens containing few types of fibers (Mazzoli et al., 2018; Lee et al., 2019; Yuan et al., 2021), for different concentrations, and sometimes, fibers of different geometries are mixed (Jung et al., 2020). Concerning fiber length, Yang et al. (2002) have carried out measurements between 2 and 18 GHz and their results show that FRC may have a frequency resonant range, depending on fiber length.

Despite these various experimental results, the engineering community is missing predictive models that would relate the SE to the characteristics of both steel fibers and concrete matrix, and design of structures is often empirical.

Meanwhile, propagation of electromagnetic waves in heterogeneous media (such as fibrous media) is a widely studied research topic. In particular, in the so-called *quasi-static regime*, separation of scales prevails (the wavelength is much greater than the size of the heterogeneities) and standard homogenization applies. In this range, many models can approximate the effective electromagnetic properties (magnetic permeability, electric permittivity and conductivity) (Maxwell Garnett, 1904; Bruggeman, 1935; Sihvola, 1999). Incidentally, these models are the electromagnetic counterpart to “mean field/effective field” (Eshelby-based) micromechanical models.

It is therefore natural to implement these models which involve fiber aspect ratio, concentration, and conductivity (real *and* imaginary parts) of both steel and concrete, and compare them to SE measurements on FRC samples.

Implementation of these models require a characterization of the concrete phase. For the time being, predicting the electromagnetic properties of concrete itself from its constituents seems to be a formidable task (Ogunsola et al., 2006; Sandrolini et al., 2007; Bourdi et al., 2012), note that concrete evolves quickly in the early months (Medeiros-Junior and Lima, 2016), which adds further complexity. In this paper, we followed an alternative route. The electromagnetic properties of concrete (without fibers) were *measured*. These measurements are then included in a predictive model of the electromagnetic properties of FRC.

The aim of this paper is threefold: (i) carry out SE measurements on FRC for various aspect ratios, concentrations, and fiber lengths, so that influence of each of these parameters can be asserted; (ii) compare measurements with the model of Maxwell Garnett (1904); (iii) identify the frequency range for which this model

applies. For engineering practices, this model will appear as a first step toward an integrated design platform, which in turn paves the way to optimization of such electromagnetic shielding systems.

The present paper is organized as follows. The experimental setup is defined in Section 2. Then, the main experimental results are revealed in Section 3. Homogenization for electromagnetic waves under the quasi-static assumption is briefly reviewed in Section 4. In particular, the model of Maxwell Garnett (1904) is presented, which predicts the effective properties of the FRC mixture from the properties of each component. Properties of concrete itself are assessed experimentally in Section 5. Predictions of the SE of FRC samples are then derived in Section 6 from the Maxwell Garnett formula and the measured properties of the cementitious matrix. The predictions are compared to measurements and several improvements of the system are suggested.

## 2. Materials and methods

### 2.1. Measurement of the shielding effectiveness

We used a steel Faraday cage by Frankonia to carry out all measurements presented below. The dimensions of the cage are:  $7.35\text{ m} \times 3.8\text{ m} \times 3.1\text{ m}$ . Samples are inserted in a  $1.2\text{ m} \times 1.2\text{ m}$  square opening located on one of the small faces of the cage. The concrete samples are poured in a steel frame which is bolted (see figs. 1–2) to the opening. A conductive gasket is placed between the two metallic frames in order to ensure electric continuity between cage and sample. Since the samples weigh about 1 t, they are moved around by means of a rolling metallic cart (see fig. 2).

Two identical bi-log type antennas (EM 6917C-1 from Electro-Metrics, see figs. 3–4) are used for the radiation measurements. The (outer) *emitting antenna* is connected to a generator (Marconi, 2022D), and an amplifier (EMC Master SA1000). The (inner) *receiving antenna* is connected to a spectrum analyzer (LG SA-7270). The antennas can be oriented vertically (see figs. 3–4) or horizontally (see fig. 6). In the former case, the resulting electromagnetic wave is polarized vertically, while in the latter case, it is polarized horizontally. Measurements are carried out at 10-20 discrete frequencies ranging from 30 MHz to 1 GHz.

The tip of the emitting antenna is placed at 1 m of the outer face of the sample. Similarly, the tip of the receiving antenna is placed at 1 m of the inner face of the sample. The thickness of all samples being 25 cm, the total (tip-to-tip) distance of the antennas is 2.25 m (see fig. 5). The receiving antenna measures the power  $\mathcal{P}_r$  of



Figure 1: A fiber-reinforced concrete sample and its metallic frame.

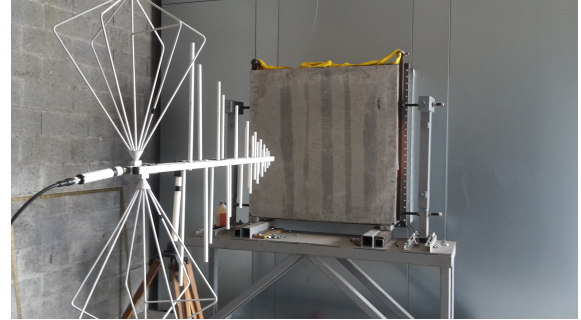


Figure 3: The emitting antenna sits outside the Faraday cage and faces the concrete sample. Because of the orientation of the antenna, the incident wave is polarized vertically.



Figure 2: A fiber-reinforced concrete sample on its rolling cart, ready to be bolted on the square opening of the Faraday cage.

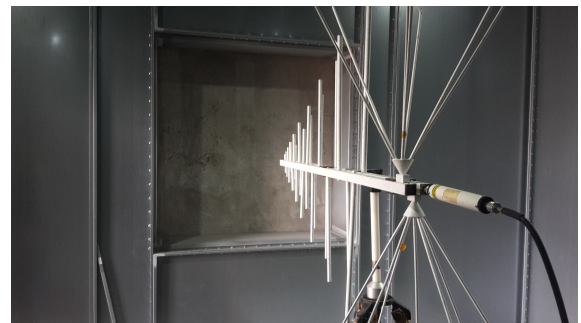


Figure 4: The receiving antenna sits inside the Faraday cage and faces the concrete sample.

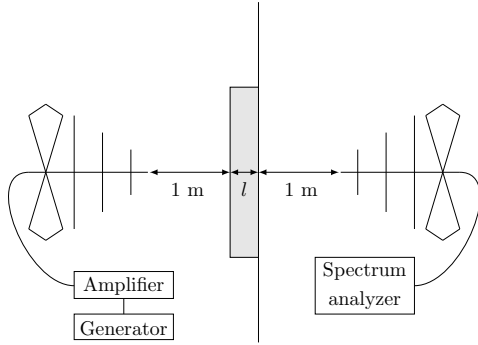


Figure 5: Sketch of our SE apparatus. The emitting (outer) antenna is connected to a generator and an amplifier. The receiving (inner) antenna is connected to a spectrum analyzer.

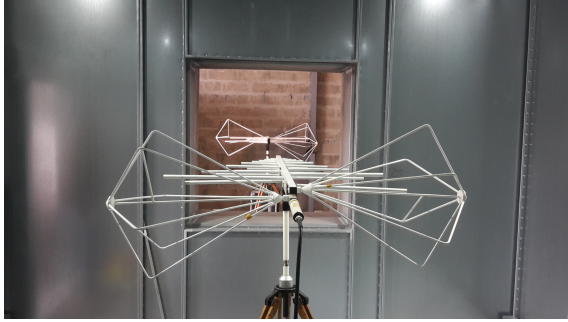


Figure 6: For the measurement of the reference value  $\mathcal{P}_i$ , the sample is removed from the Faraday cage. On this picture, the emitting is horizontal: therefore, the incident wave is polarized horizontally.

the electromagnetic wave sent by the emitting antenna and transmitted by the sample.

Concurrently, a reference measurement is performed: both antennas are kept in the same configuration, while the sample is removed from the square opening (see fig. 6). The receiving antenna measures the electromagnetic power  $\mathcal{P}_i$  of the incident wave, without shielding. Transmission coefficient  $\tau$  and the shielding effectiveness SE (in decibels) are then given by:

$$\tau = \frac{\mathcal{P}_r}{\mathcal{P}_i} \quad \text{and} \quad \text{SE}_{\text{dB}} = -10 \log_{10} \tau. \quad (1)$$

## 2.2. Description of the samples

Fourteen FRC blocks (see table 1) and one plain concrete block were tested in this study. The dimensions of each block were:  $1.2 \text{ m} \times 1.2 \text{ m} \times 0.25 \text{ m}$  (total weight: about 900 kg).

The plain concrete block and ten out of the fourteen FRC blocks were obtained from the same premix (*Betomur*, C20/25, CEM II/C from Cantillana). A different,



Figure 7: From left to right: fibers of type 80/60, 65/35, 80/30, 45/30 and 62/13.

Fiber type	Mass content [ $\text{kg}/\text{m}^3$ ]			
	20	40	60	100
62/13	12 <sup>†</sup>	12, 173	12 <sup>†</sup>	X
45/30	13 <sup>†</sup>	X	13 <sup>†</sup>	X
80/30	9	9, 150	9, 90	35
65/35	12, 173	12, 170	12, 90	X
80/60	7, 27, 41	49	X	X

Table 1: Overview of the various FRC samples that were tested in this study. Rows correspond to various types of fibers, while columns correspond to various mass contents of fibers. In each cell, the age (days) at testing is indicated (“X” means “not tested”). The dagger † symbol marks samples that were cast from the t-mix premix.

but similar premix was used for the four remaining samples (*Béton Standard*, C25/30 from t-mix).

Various types of steel fibers were tested. Since these fibers are intended as structural reinforcement, they are not straight; rather, they exhibit hooked ends (see fig. 7). In this study, we discard these geometric details and focus on the main geometric parameters: the total length of the fibers  $a$  and their aspect ratio  $e = a/d$  ( $d$ : diameter). For the sake of conciseness, fibers will be referred to as the pair  $e/a$  (for example, the fiber referred to as “80/30” has an aspect ratio of  $e = 80$ , while its total length is  $a = 30 \text{ mm}$ ). Five types of fibers were tested: 62/13, 45/30, 80/30, 65/35, 80/60 at four values of the mass content: 20, 40, 60 and  $100 \text{ kg}/\text{m}^3$ . Most samples were tested at a rather early age (about ten days after casting). In order to assess the evolution of the shielding effectiveness with time, measurements at a later age were also performed. For each fiber reinforced sample, table 1 displays the type of fibers, their mass content, and the age at testing. The plain concrete sample was tested at 6, 16, 26, 40, 61, 76 and 191 days after casting.

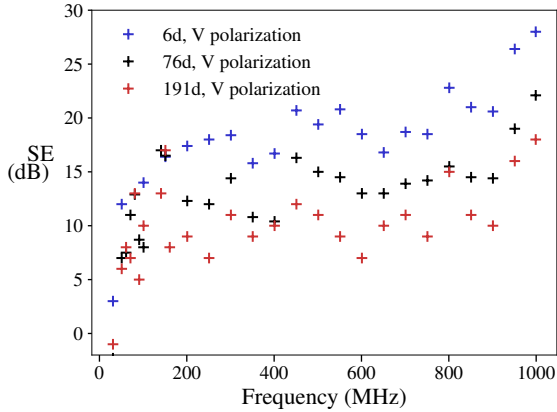


Figure 8: Shielding effectiveness of the plain concrete sample at 6, 76 and 191 days. The plots refer to electromagnetic waves that were polarized vertically (both antennas are oriented vertically).

### 3. Experimental results

Fig. 8 shows the measured shielding effectiveness of the plain concrete sample at 6, 76 and 191 days. Two general trends can be identified: (1) SE is higher at high frequencies and (2) SE decreases with time. The latter shows that concrete is not an inert material: both its structure and chemistry evolve over a long period of time.

Fig. 9 now shows the measured shielding effectiveness of 45/30 fibers at 13 days, for waves that are polarized vertically and horizontally. Both polarizations lead to SE curves that are very similar: in the remainder of this paper, we will report results on vertically polarized incident waves only. Like plain concrete, SE increases with frequency, reaching nearly 80 dB at 1 GHz, vs. less than 30 dB for plain concrete. As expected, SE also increases with the fiber content.

Note that differences between the two polarizations can be explained by the fact that the cross-section of the Faraday cage is not square and the horizontal and vertical directions play slightly different roles. This shows that the proposed experimental measurement of the SE is not intrinsic to the FRC block itself: rather, the measured SE characterizes the whole system block + cage. In Sec. 6, no attempt has been made at correcting for the boundary effects induced by the cage in.

Fig. 10 now shows the measured SE of blocks reinforced with 80/30 fibers at 9 d. Again, SE increases with frequency and fiber content. Comparison of Figs. 9 and 10 shows that for identical fiber length ( $a = 30$  mm) and fiber content (20 and 60 kg/m<sup>3</sup>) and similar ages (13 d vs. 9 d), the shielding effectiveness of the 80/30 block is

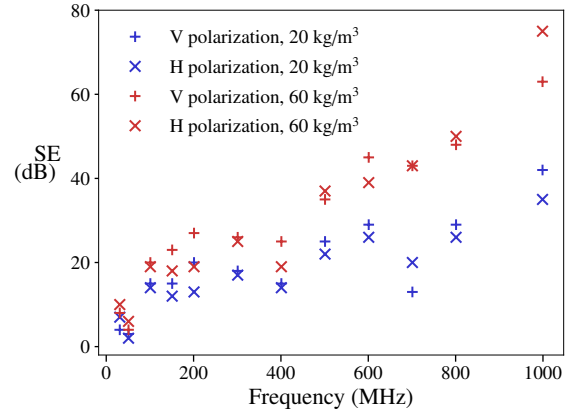


Figure 9: Shielding effectiveness of the blocks reinforced with fibers 45/30 at 13 d, for various mass contents (20 and 60 kg/m<sup>3</sup>) and for vertically and horizontally polarized incident waves.

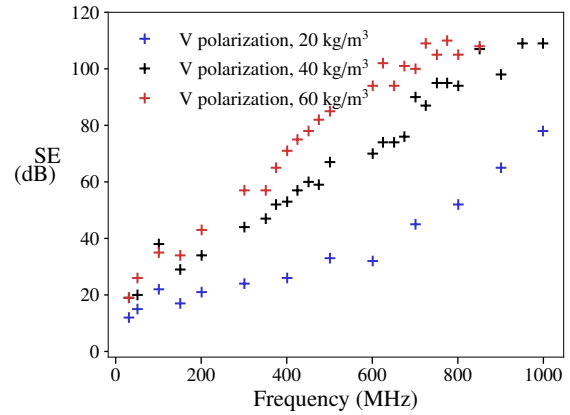


Figure 10: Shielding effectiveness of the blocks reinforced with fibers 80/30 at 9 d for various mass contents (20, 40 and 60 kg/m<sup>3</sup>) and vertically polarized incident waves.

significantly higher than the 45/30 block. Slender fibers thus seem to be more efficient.

To close this section, the shielding effectiveness at early (12 d) and later (90, 170, 173 d) ages is plotted in Figs. 11 and 12 for fiber 65/35. Like plain concrete, SE clearly decreases over time.

Note that further experimental results (for fibers 62/13 and 80/60) can be found in Sec. 6. Overall, the highest SE reached at high frequencies is about 130 dB (for fiber 80/30 at 100 kg/m<sup>3</sup>). Below 200 MHz, however, the SE is rarely above 40 dB.

### 4. Theoretical background

Our goal is to develop a simple predictive model of the shielding effectiveness of a fiber reinforced concrete

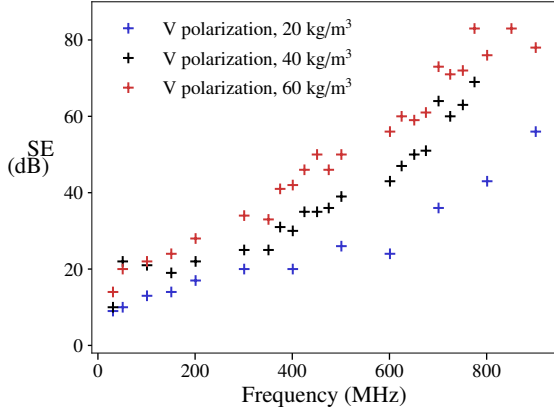


Figure 11: Shielding effectiveness of the blocks reinforced with fibers 65/35 at 12 d for various mass contents (20, 40 and 60 kg/m<sup>3</sup>) and vertically polarized incident waves.

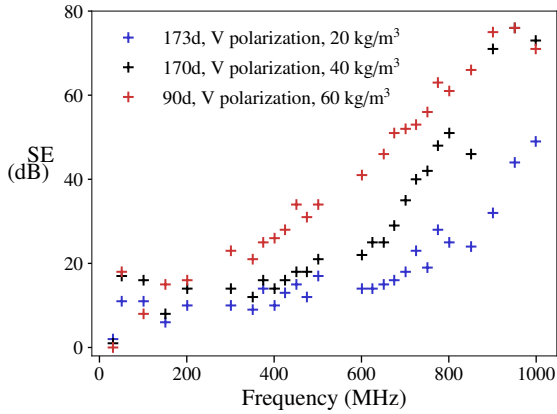


Figure 12: Shielding effectiveness of same blocks as in Fig. 11 at a later age (90, 170, 173 d).

wall. Ideally, this model would take the concrete formulation and the properties of the steel fibers as an input. However, predicting the conductivity of concrete from its constituents is a formidable task.

As a first step, we propose in this paper a model that takes as input the electromagnetic and geometric properties of the steel fibers *and* the electromagnetic properties of concrete. The latter is *measured* from an inverse analysis of our SE measurements of the plain concrete block (see Sec. 5). This analysis relies on the closed-form expression of the shielding effectiveness of homogeneous, infinite walls, presented in Sec. 4.1. Of course, the plain concrete sample considered in this study is neither infinite, nor homogeneous. Still, the heterogeneities are small compared to the thickness of the wall, while its width is large compared to the thickness. We therefore assume that formula (2) applies.

Our proposed prediction of the shielding effectiveness of FRC walls then proceeds in two steps. Under the quasi-static assumption stated in Sec. 4.2, the effective electromagnetic properties of the concrete + fibers mixture are first estimated by means of the Maxwell Garnett model introduced in Sec. 4.3. Then, we use again the formula of Sec. 4.1 to evaluate the shielding effectiveness.

#### 4.1. Shielding effectiveness of a homogeneous, infinite wall

We consider an infinite wall made of an isotropic homogeneous material  $\mathcal{M}$  and surrounded by vacuum. The electromagnetic constants of material  $\mathcal{M}$  are its magnetic permeability  $\mu$ , its dielectric permittivity  $\epsilon$  and its conductivity  $\sigma$ ; the electromagnetic constants of vacuum are:  $\mu_0$  (magnetic permeability) and  $\epsilon_0$  (permittivity). The thickness of the wall is  $l$ .

An electromagnetic incident wave propagates in vacuum, perpendicularly to the wall and hits the wall. Upon traversing the wall, the wave is attenuated. The resulting shielding effectiveness SE [as defined by Eq. (1)] is a classical result of electromagnetic compatibility (Paul, 2006; Ott, 1988)

$$SE = -20 \log \left| e^{jkl} \frac{4\eta\eta_0}{(\eta_0 + \eta)^2 e^{2jkl} - (\eta_0 - \eta)^2} \right|, \quad (2)$$

where  $\eta = \mathcal{H}(\mu, \epsilon, \sigma)$  and  $\eta_0 = \sqrt{\mu_0/\epsilon_0}$  are the so-called electromagnetic *impedance* of the material  $\mathcal{M}$  and of vacuum, respectively. Besides,  $k = 2\pi f\mu/\eta$  is the wave-number for propagation in the material at the frequency  $f$  of the incident wave. Note that both  $\eta$  and  $k$  are complex numbers. The reader is referred to Appendix A for a closed-form expression of  $\mathcal{H}$ , that relates the impedance to the electromagnetic constants.

#### 4.2. The quasi-static assumption

Formula (2) was derived for *homogeneous* materials. It does not apply to *heterogeneous* materials such as FRC. This limitation can be circumvented under the classical assumption that *scales are separated* (the so-called *quasi-static assumption*). In the present case we require the size of the heterogeneities (the length of the fibers) to be small compared to the wavelength *and* the thickness  $l$  of the wall.

Under this assumption, the heterogenous material can be homogenized as an effective material. For fibers distributed isotropically, the effective electromagnetic material is also isotropic, with (scalar) electromagnetic constants:  $\mu_{\text{eff}}$ ,  $\epsilon_{\text{eff}}$  and  $\sigma_{\text{eff}}$ . The values of these effective constants the values of which are derived from the solution to three so-called *local problems* (or *corrector problems*) formulated over the *Representative Volume Element* (RVE), see Appendix B.

Then, the shielding effectiveness of the FRC wall can be estimated from Eq. (2) upon substitution of  $\mu$ ,  $\epsilon$  and  $\sigma$  with  $\mu_{\text{eff}}$ ,  $\epsilon_{\text{eff}}$  and  $\sigma_{\text{eff}}$ .

Does the quasi-static assumption hold in the present case? From Tab. 1, it is seen that the maximum length of the fibers is  $a = 60$  mm, while the thickness of the wall is  $l = 250$  mm. Therefore,  $a/l \approx 0.24$ , which is usually small enough for homogenization to apply. However, it should also be verified that  $a \ll \lambda_{\text{eff}}$ , where  $\lambda_{\text{eff}}$  is the *effective* wavelength. Since  $\lambda_{\text{eff}}$  is not known yet, this verification is deferred until Sec. 7. Note that longer wavelengths means smaller frequencies. Therefore, the quasi-static assumption should be understood as a low-frequency assumption.

#### 4.3. The Maxwell Garnett model

In order to apply Eq. (2) to a FRC wall, the effective electromagnetic constants of the heterogeneous material must first be estimated. In theory, this requires the solutions to the local problems defined in Appendix B, which is too costly. For low volume fractions of inclusions, mean-field models generally deliver satisfactory estimates of the effective properties, and we will resort to the classical model of Maxwell Garnett (1904) (see also Sihvola, 1999), which was later adapted to prolate ellipsoidal inclusions (Stratton, 1941; Sihvola, 1999). Note that this model is analogous to the Mori–Tanaka model in micromechanics (?).

These mean-field models rely on the solution to the problem of a single inclusion embedded in an infinite matrix, subjected to a remote electric field (or remote strain), as depicted in Fig. 13. This problem is known as Laplace’s problem in electromagnetism Stratton (1941)

and Eshelby’s problem in mechanics Eshelby (1957). Closed-form solutions are available for both problems, provided that the inclusion is ellipsoidal. We will therefore approximate the cylindrical fibers with prolate ellipsoids (with same aspect ratio  $e$ ).

Before the Maxwell Garnett problem is presented, let us note that, as a first step toward a full electromagnetic model of FRC walls, we have discarded the homogenization of the magnetic permeability, by assuming that both steel fibers and concrete matrix have the same magnetic permeability as the vacuum,  $\mu_0$ . The effective magnetic permeability of FRC is therefore also isotropic, and  $\mu_{\text{eff}} = \mu_0$ . We are therefore left with the determination of *two* constants only. Both can in fact be found simultaneously from the homogenization of the *complex permittivity*  $\epsilon - j\sigma/\omega$ . In the remainder of this section, all formulas are expressed in terms of the complex permittivity, which, for the sake of simplicity, will be again denoted  $\epsilon$ .

We therefore consider a two-phase material made up of ellipsoidal inclusions (aspect ratio:  $e$ ; volume fraction:  $\phi$ ; complex isotropic permittivity:  $\epsilon_i$ ) embedded in a homogeneous matrix (complex isotropic permittivity:  $\epsilon_m$ ). The homogenized complex permittivity is then given by

$$\frac{\epsilon_{\text{eff}}}{\epsilon_m} = \mathbf{I} + \zeta\phi [\mathbf{I} - \zeta\phi\langle\mathbf{M}(\mathbf{n}) \cdot \mathbf{N}(\mathbf{n})\rangle]^{-1} \cdot \langle\mathbf{M}(\mathbf{n})\rangle, \quad (3)$$

where  $\mathbf{I}$  is the second-order identity tensor,  $\langle\bullet\rangle$  denotes the average over all possible orientations  $\mathbf{n}$  (unit vector) of the ellipsoidal inclusions, and  $\zeta = (\epsilon_i - \epsilon_m)/\epsilon_m$ . The second-order tensors  $\mathbf{M}(\mathbf{n})$  and  $\mathbf{N}(\mathbf{n})$  are defined as follows, for any unit vector  $\mathbf{n}$

$$\mathbf{M}(\mathbf{n}) = [\mathbf{I} + \zeta\mathbf{N}(\mathbf{n})]^{-1}, \quad (4)$$

$$\mathbf{N}(\mathbf{n}) = N_1(\mathbf{I} - \mathbf{n} \otimes \mathbf{n}) + N_3\mathbf{n} \otimes \mathbf{n}, \quad (5)$$

with

$$N_1 = N_2 = \frac{1}{2}(1 - N_3), \quad (6)$$

$$N_3 = \frac{1 - \chi^2}{2\chi^3} \left( \ln \frac{1 + \chi}{1 - \chi} - 2\chi \right), \quad \chi = \sqrt{1 - \frac{1}{e^2}}. \quad (7)$$

For isotropically distributed inclusions, the effective complex permittivity is also isotropic,  $\epsilon_{\text{eff}} = \epsilon_{\text{eff}}\mathbf{I}$  is isotropic, and Eq. (3) becomes

$$\frac{\epsilon_{\text{eff}}}{\epsilon_m} = 1 + \frac{\frac{\zeta\phi}{3} \sum_{j=1,2,3} (1 + \zeta N_j)^{-1}}{1 - \frac{\zeta\phi}{3} \sum_{j=1,2,3} N_j (1 + \zeta N_j)^{-1}}. \quad (8)$$

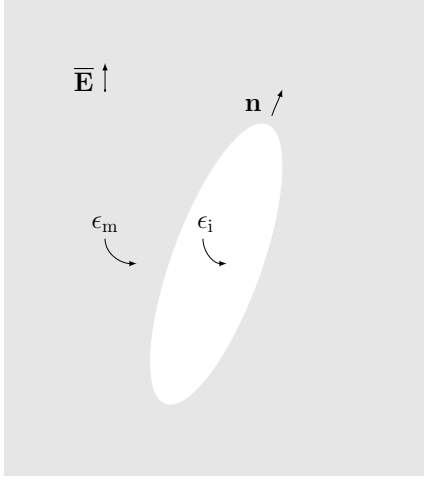


Figure 13: Laplace's problem: a single (spheroidal) inclusion (complex permittivity:  $\epsilon_i$ ) is embedded in an infinite, homogeneous matrix (complex permittivity:  $\epsilon_m$ ) and subjected to a remote electric field  $\vec{E}$ . The unit vector  $\mathbf{n}$  denotes the orientation of the axis of the inclusion.

For inclusions with large complex conductivity  $|\epsilon_i| \gg |\epsilon_m|$ , we have  $|\zeta| \rightarrow +\infty$  and

$$\frac{\epsilon_{\text{eff}}}{\epsilon_m} = 1 + \frac{\phi}{3(1-\phi)} \sum_{j=1,2,3} N_j^{-1}. \quad (9)$$

## 5. Characterization of the plain concrete block

The SE measurements of the plain concrete block are displayed in Fig. 8. In this section, we invert Eq. (2) to retrieve the complex permittivity  $\epsilon_c - j\sigma_c/\omega$  of plain concrete, where  $\epsilon_c$  is the real permittivity and  $\sigma_c$  is the conductivity (it is recalled that we assumed  $\mu_c \approx \mu_0$ ). Of course, measuring the SE (real scalar) does not suffice to determine *both* real *and* imaginary parts of the complex permittivity.

To overcome this limitation, observing that the conductivity is the dominant parameter, we *fix the permittivity*  $\epsilon_c$ . Then, the conductivity  $\sigma_c$  is defined unequivocally by the value of SE. As suggested by our SE measurements, we assume that the permittivity of concrete is interpolated linearly between the following values

$$\epsilon_c(t = 6 \text{ d}) = 13\epsilon_0 \quad \text{and} \quad \epsilon_c(t = 40 \text{ d}) = 3\epsilon_0, \quad (10)$$

$\epsilon_c$  being constant after 40 d. These somewhat arbitrary values are consistent with the measurements of [Guihard \(2018\)](#) for various saturation degrees. It will be further shown in Sec. 6, that our model exhibits low sensitivity to permittivity.

The conductivities obtained from the inversion of Eq. (2) are presented in Figs. 14 and 15. It is observed

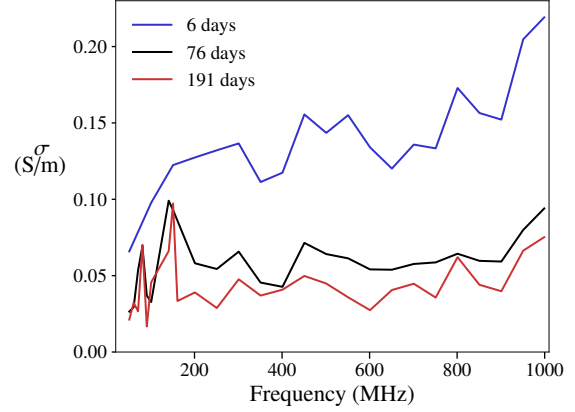


Figure 14: Electric conductivity of plain concrete at 6 d, 76 d and 191 d. The inverse analysis described in Sec. 5 has been applied to the measurements shown in Fig. 8.

that the conductivity reduces significantly with time. This is readily understood from the observation that the electromagnetic properties of concrete highly depend on the interstitial solution that partially saturates its porous network ([Khadra et al., 2017](#); [Snyder et al., 2003](#); [Vollpracht et al., 2016](#)). The chemical composition of this solution evolves with time because of the slow kinetics of the hydration reaction. Besides, interactions with the surrounding environment can affect the saturation degree. Accounting for these effects is outside the scope of the present study.

## 6. Assessment of our SE model

In this section, we compare the SE measurements of FRC blocks with estimates given by the Maxwell Garnett introduced in Sec. 4.3. In the present case, the matrix “m” is concrete, while the inclusions “i” are the steel fibers

$$\epsilon_m = \epsilon_c - j\sigma_c/\omega \quad \text{and} \quad \epsilon_i = \epsilon_s - j\sigma_s/\omega, \quad (11)$$

with

$$\sigma_s = 10^7 \text{ S/m} \quad \text{and} \quad \epsilon_s = \epsilon_0. \quad (12)$$

Note that the conductivity  $\sigma_s$  of steel is so high that the precise value of its permittivity does not matter (we chose  $\epsilon_0$ ). Formula (8) then delivers the complex permittivity  $\epsilon_{\text{FRC}} - j\sigma_{\text{FRC}}/\omega$  of FRC (we assume that the fibers are distributed isotropically in the samples; this leads to an isotropic effective material). Finally, formula (2) is applied to compute the shielding effectiveness of the FRC wall.

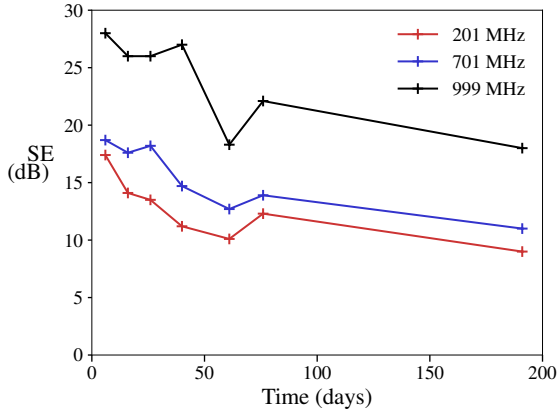


Figure 15: Electric conductivity of plain concrete over the whole time-frame, at 201 MHz, 701 MHz and 999 MHz. The inverse analysis described in Sec. 5 has been applied to the measurements shown in Fig. 8.

Note that all samples were analysed neither at exactly the same age, nor for exactly the same frequencies. When necessary, the concrete permittivities and conductivities were therefore interpolated linearly with respect to time (between 6, 16, 26, 40, 61, 76 and 191 days) and to frequencies.

Fig. 16 displays the experimental values and theoretical predictions of the shielding effectiveness of concrete samples reinforced with fibers of type 62/13 at 12 d for the following mass contents:  $20 \text{ kg/m}^3$  and  $60 \text{ kg/m}^3$ . Fig. 18 displays these values for the same type of fibers, at  $40 \text{ kg/m}^3$  and at 12 and 173 d. In both figures, the frequencies are displayed on a logarithmic scale, so as to highlight the low frequencies.

In Sec. 5, the permittivity of concrete was *postulated* [see Eq. (10)]. In Figs. 16 and 18, the permittivity of concrete was varied from  $\epsilon_0$  to  $20\epsilon_0$ , delivering the shaded areas surrounding the continuous lines. It is observed that our model exhibits a low sensitivity to the actual value of  $\epsilon_c$ .

Overall, these plots show that experimental measurements and model predictions are in excellent agreement at low frequencies. As expected, divergence occurs at high frequencies. It is important to note that the validity range of our model *depends on the fiber content and on the sample's age* (see Sec. 7). At  $20 \text{ kg/m}^3$  and 12 d (see Fig. 16), the agreement is excellent over the whole range of frequencies. At  $60 \text{ kg/m}^3$  and 12 d (see Fig. 16), the model is valid for frequencies lower than 200 MHz. At  $40 \text{ kg/m}^3$  and 12 d (resp. 173 d) the frequency must remain below 300 MHz (resp. 500 MHz).

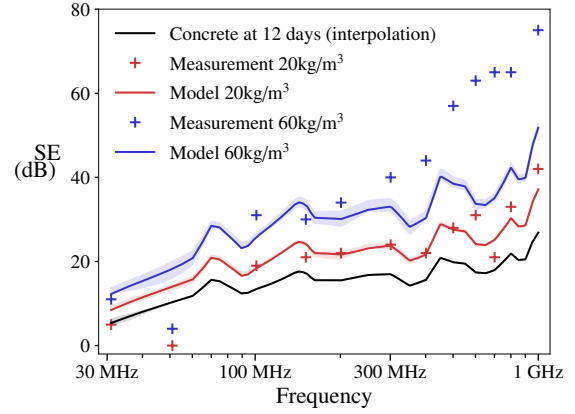


Figure 16: Experimental measurement and theoretical predictions of the shielding effectiveness of fiber 62/13 at 12 d. At  $20 \text{ kg/m}^3$ , the agreement is excellent over the whole range of frequencies. At  $60 \text{ kg/m}^3$ , our model becomes inaccurate at about 200 MHz.

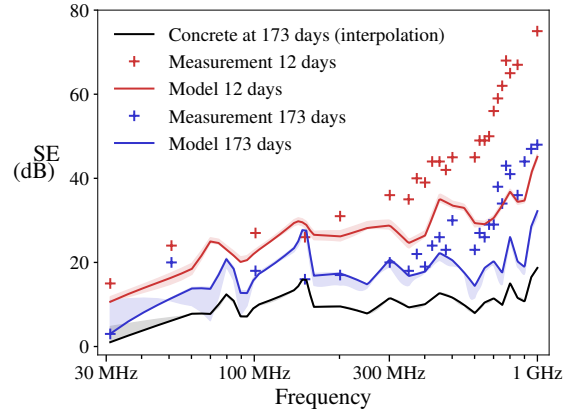


Figure 17: Experimental measurement and theoretical predictions of the shielding effectiveness of fiber 62/13 at  $40 \text{ kg/m}^3$ . At 12 d, our model is valid for frequencies lower than 300 MHz; at 173 d, the upper limit is 500 MHz.

Figure 18: Comparison model/measurement, fiber 62/13,  $40 \text{ kg/m}^3$

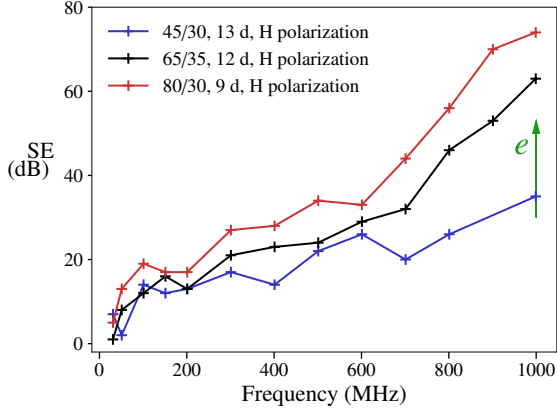


Figure 19: Influence of aspect ratio on shielding effectiveness. We compare 3 blocks that were tested at approximately the same time. The fibers have approximately the same length and the mass content is  $20 \text{ kg/m}^3$ . Clearly, the SE increases with the aspect ratio  $e$ .

To close this section, we highlight the influence of the aspect ratio of fibers. Our model predicts that, at constant mass content, increasing the slenderness of the fibers increases the shielding effectiveness. This is confirmed by our measurements. Figs. 19 and 20 show the shielding effectiveness of fibers with aspect ratios 45, 65 and 80, age, length and mass content being fixed. Clearly, SE increases with slenderness. Although our model does not apply in this range, it seems that this result carries to high frequencies too.

## 7. Validity of the quasi-static assumption

As explained in Sec. 4.2, the quasi-static approximation is valid for low values of the ratio  $a/\lambda_{\text{FRC}}$  only, where  $a$  denotes the fiber length, while  $\lambda_{\text{FRC}}$  refers to the wavelength in the FRC block, at frequency  $f$ . It is related to the effective electromagnetic constants  $\epsilon_{\text{FRC}}$  and  $\sigma_{\text{FRC}}$  through the following formulas (see Appendix A)

$$\lambda_{\text{FRC}} = \frac{1}{f \sqrt{\mu_0 \alpha_{\text{FRC}}}}, \quad (13)$$

where

$$\alpha_{\text{FRC}} = \sqrt{\frac{\epsilon_{\text{FRC}} + \sqrt{\epsilon_{\text{FRC}}^2 + \sigma_{\text{FRC}}^2 / \omega^2}}{2}}. \quad (14)$$

However, the true values of  $\epsilon_{\text{FRC}}$  and  $\sigma_{\text{FRC}}$  are not known for our FRC samples. Since we want to assess the validity of our model, we ought not to use the Maxwell Garnett estimates of these quantities. We propose an alternative inverse analysis, that is based on the

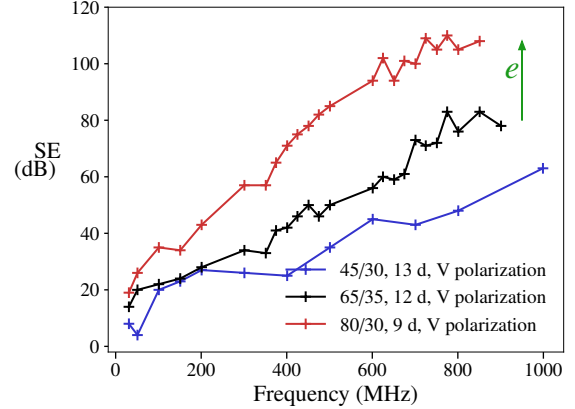


Figure 20: Influence of aspect ratio on shielding effectiveness. We compare 3 blocks that were tested at approximately the same time. The fibers have approximately the same length and the mass content is  $60 \text{ kg/m}^3$ . Clearly, the SE increases with the aspect ratio  $e$ .

observation that, for highly conductive fibers at low frequencies, the complex permittivity of FRC is equal to the complex permittivity of plain concrete, *scaled by a real factor  $\gamma$*  [Eq. (9) provides the Maxwell Garnett estimate of the  $\gamma$  factor].

Our analysis relies on the assumption that this result remains true at intermediate frequencies (when the quasi-static assumption begins to fail). In other words, we assume that for frequencies  $f$  “not too large” (in a sense that will be clarified below), there exists a real factor  $\gamma$  such that

$$\sigma_{\text{FRC}} = \gamma \sigma_c \quad \text{and} \quad \epsilon_{\text{FRC}} = \gamma \epsilon_c, \quad (15)$$

where  $\gamma$ ,  $\epsilon_c$ ,  $\sigma_c$ ,  $\epsilon_{\text{FRC}}$ ,  $\sigma_{\text{FRC}}$  all depend on the frequency  $f$ . Since  $\sigma_c$  and  $\epsilon_c$  have already been determined experimentally at all frequencies (see Sec. 5), we are left with the determination of a single real scalar  $\gamma$ . Eq. (2) now delivers a *unique* value of  $\gamma$ . Finally, the wavelength  $\lambda_{\text{FRC}}$  results from the application of Eqs. (13).

The results of this analysis are shown in Figs. 21 and 22 for three types of fibers. In these figures,  $\gamma$  is plotted vs.  $a/\lambda_{\text{FRC}}$ . It is remarkable that all curves show a similar trend: a low frequency plateau, where  $\gamma$  coincides with its Maxwell Garnett estimate (9), is followed by a high frequency regime, where  $\gamma$  increases significantly. The two regimes are delimited by a ratio  $a/\lambda_{\text{FRC}}$  situated between 0.1 and 0.15. This trend is observed for all other types of fibers, which are not presented here for the sake of conciseness.

This analysis therefore suggests that the quasi-static assumption is valid for  $a/\lambda_{\text{FRC}} \leq 0.15$ . This criterion is consistent with Figs. 16 and 18, where, *for*

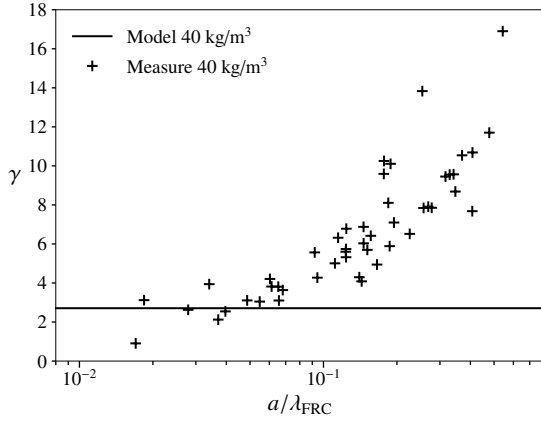


Figure 21: Values of the  $\gamma$  ratio defined in Sec. 7, for fiber 62/13 at  $40 \text{ kg/m}^3$ . Note that this plot aggregates the measurements at 12 and 173 d.

the same type of fibers, the upper limit of the quasi-static range was found to depend on age ( $\lambda_{\text{FRC}}$  increases with time) and fiber content ( $\lambda_{\text{FRC}}$  decreases for larger volume fractions). It is also consistent with the limit  $a/\lambda_{\text{FRC}} \leq 1/(2\pi) \approx 0.16$  that is often proposed in the literature (see for example (see for example Sihvola, 1999, §8.1.2)).

To close this section, it is observed that when  $a/\lambda_{\text{FRC}}$  is “not small”, then this ratio becomes a new parameter of the problem. In other words, like in the low-frequency regime, the shielding effectiveness depends on the aspect ratio  $e$  of the fibers. Unlike in the low-frequency regime, it also depends on the length of the fibers. Observation of Figs. 23 and 24, where two fibers with same slenderness  $e = 80$  and different sizes  $a = 30, 60 \text{ mm}$  are compared, seems to indicate that increasing the length  $a$  of the fibers, tends to improve the shielding effectiveness. From the perspective of material optimization, this is a valuable qualitative information.

## 8. Conclusion and outlook

In this paper, we have reported experimental measurements of the shielding effectiveness (SE) of fiber reinforced concrete samples. Tests were performed in a large Faraday cage, for frequencies ranging from 30 MHz to 1 GHz. The values of both the permittivity and conductivity of concrete have been found by an inverse analysis of the measured shielding effectiveness of a plain concrete sample. Then, plugging these values into the Maxwell Garnett model, a prediction of the shielding effectiveness of fiber-reinforced concrete was

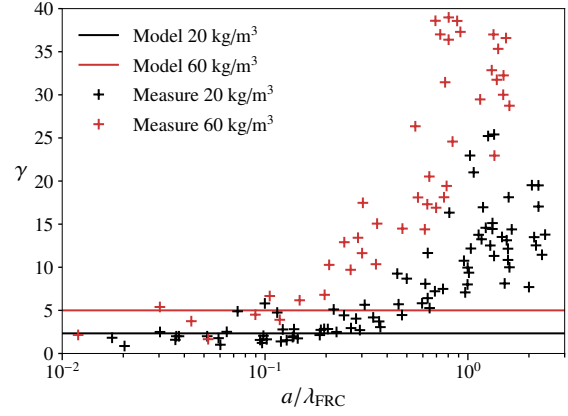


Figure 22: Values of the  $\gamma$  ratio defined in Sec. 7, for fibers 80/30 and 80/60 at 20 and  $60 \text{ kg/m}^3$ . Note that this plot aggregates all available measurements, at early and later ages.

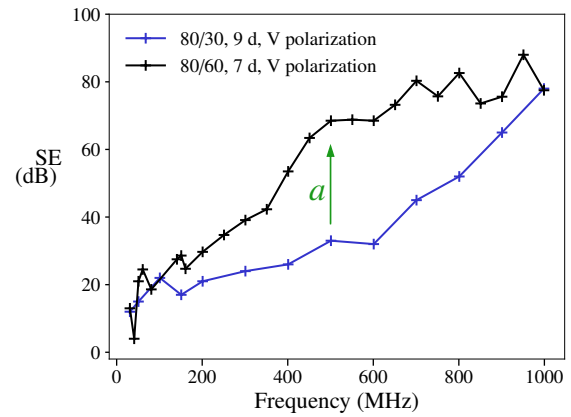


Figure 23: Shielding effectiveness at early age of two types of fibers, 80/30 and 80/60, that share the same aspect-ratio  $e = 80$ , but have different lengths  $a = 30 \text{ mm}$  and  $a = 60 \text{ mm}$ . The fiber mass content is  $20 \text{ kg/m}^3$ . At high frequencies, longer fibers seem to be beneficial.

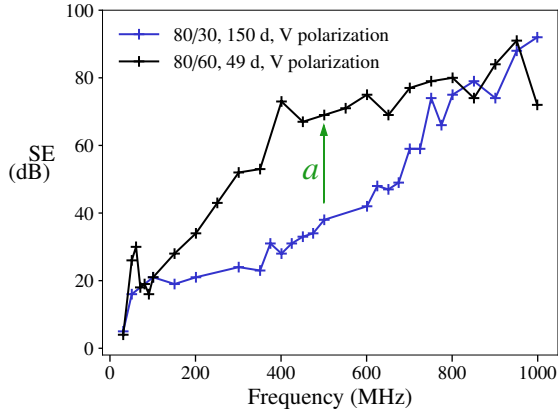


Figure 24: Shielding effectiveness at a later age of two types of fibers, 80/30 and 80/60, that share the same aspect-ratio  $e = 80$ , but have different lengths  $a = 30$  mm and  $a = 60$  mm. The fiber mass content is  $40 \text{ kg/m}^3$ . At high frequencies, longer fibers seem to be beneficial.

obtained and compared to the measurements. Excellent agreement is generally observed in the low-frequency regime, while at high-frequencies, our model underestimates the shielding effectiveness. Besides, we were able to quantify what “low-frequency” actually means.

An important practical result of this work is that, for frequencies such that  $a/\lambda_{\text{FRC}} \leq 0.15$ , the Maxwell Garnett model is an appropriate design tool for the engineering community.

Our experiments and modelling have revealed several additional facts. First, the shielding effectiveness of concrete (plain or reinforced) samples decreases over time. Second, higher aspect ratios are favorable to the shielding effectiveness over the whole range of frequencies. Third, at high frequencies, longer fibers seem to be preferable.

This work opens several perspectives, both theoretical and practical. From the point of view of homogenization theory, it should be noted that the Maxwell Garnett model is valid for low volume fractions only. We have not questioned this hypothesis in our study. Because of the good agreement that we observed between our measurements and our predictions, we can safely assume that interactions between fibers remain small, even at  $60 \text{ kg/m}^3$ . This would certainly no longer be true at higher mass contents and ought to be investigated in future work. Besides, for ratios  $a/\lambda_{\text{FRC}}$  greater than 0.15, the quasi-static assumption is no longer applicable, and other upscaling techniques should be used. At intermediate frequencies  $a \approx \lambda_{\text{FRC}}$ , higher-order material models could be investigated. Investigating the domain  $a \gg \lambda_{\text{FRC}}$  is also an exciting perspective.

From the point of view of the concrete material itself, this work raises two important practical issues. First, the smallest fibers considered in this work are comparable with the size of the largest aggregates. Interaction between fibers and aggregates or interstitial solution contained in the largest pores should therefore be investigated. Finally, our measurements were carried out over a relatively short period of time (about 6 months). This study should be extended to a much longer period of time (several years) in order to assess the shielding effectiveness over the lifetime of a structure. It should also account for interactions with the environment (variations of relative humidity in particular).

### CRediT authorship contribution statement

**A. Martin:** Conceptualization, Investigation, Methodology, Validation, Visualization, Writing – original draft. **S. Brisard:** Conceptualization, Project administration, Resources, Supervision, Writing – review & editing. **K. Sab:** Conceptualization, Funding acquisition, Resources, Writing – review & editing. **S. Ben Mbarek:** Investigation, Writing – review & editing. **J. P. Caron-Fellens:** Investigation, Resources, Writing – review & editing.

### Declaration of competing interest

The authors declare that they have no known competing financial interests or personal relationships that could have appeared to influence the work reported in this paper.

### Data availability

Data will be made available on request.

### Acknowledgments

We acknowledge *Spie batignolles génie civil* and EuroMC for providing financial resources to this work.

### A. Propagation of plane waves in homogeneous, isotropic materials

We consider a homogeneous, infinite medium with electromagnetic constants  $\mu$ ,  $\epsilon$  and  $\sigma$ . A plane wave propagates along the  $z > 0$  direction. Considering an electromagnetic plane wave propagating along  $z$  direction. The electric field then reads

$$\mathbf{E} = E_0 e^{-j(kz - \omega t)} \mathbf{e}_y \quad (\text{A.1})$$

where  $k$  is the wave number,  $\omega = 2\pi f$  is the pulsation ( $f$ : frequency) and  $E_0$  is the complex amplitude ( $\mathbf{e}_y$  is defined as the constant direction of  $\mathbf{E}$ ). Plugging this expression into the wave equation

$$\mathbf{rot rot E} = \omega^2 \mu (\epsilon - j\sigma/\omega) \mathbf{E}, \quad (\text{A.2})$$

it is found that

$$k^2 = \omega^2 \mu (\epsilon - j\sigma/\omega). \quad (\text{A.3})$$

For a wave that propagates in the  $z > 0$  direction, the real part of  $k$  must be positive. Therefore, the wave-number  $k$  and wave-length  $\lambda$  read

$$k = \omega \sqrt{\mu} (\alpha + j\beta) \quad \text{and} \quad \lambda = \frac{1}{f \sqrt{\mu} \alpha}, \quad (\text{A.4})$$

where

$$\alpha = \sqrt{\frac{\epsilon + \sqrt{\epsilon^2 + \sigma^2/\omega^2}}{2}} \quad \text{and} \quad \beta = -\frac{\sigma}{2\alpha\omega}. \quad (\text{A.5})$$

The *electromagnetic impedance* is then defined as the following quantity

$$\eta = \sqrt{\mu} / (\alpha + j\beta). \quad (\text{A.6})$$

## B. Homogenization under the quasi-static assumption

The literature on this topic is very large (see for example Sihvola, 1999; Artola and Cessenat, 1990; Sanchez-Palencia and Sanchez-Hubert, 1978; Canot and Frénod, 2017). Using two-scale convergence in particular, Canot and Frénod (2017), Wellander (2001) and Sanchez-Palencia (1980) have proved that the heterogeneous material behaves as an effective material that follows the macroscopic Maxwell equations

$$\mathbf{rot E}_{\text{eff}} = -j\omega \mathbf{B}_{\text{eff}}, \quad (\text{B.1})$$

$$\mathbf{rot H}_{\text{eff}} = \mathbf{J}_{\text{eff}} + j\omega \mathbf{D}_{\text{eff}}, \quad (\text{B.2})$$

where:

$$\mathbf{D}_{\text{eff}} = \epsilon_{\text{eff}} \cdot \mathbf{E}_{\text{eff}} \quad (\text{B.3})$$

$$\mathbf{J}_{\text{eff}} = \sigma_{\text{eff}} \cdot \mathbf{E}_{\text{eff}} \quad (\text{B.4})$$

$$\mathbf{H}_{\text{eff}} = (\boldsymbol{\mu}_{\text{eff}})^{-1} \cdot \mathbf{B}_{\text{eff}} \quad (\text{B.5})$$

The effective electromagnetic properties  $\epsilon_{\text{eff}}$ ,  $\sigma_{\text{eff}}$  and  $\boldsymbol{\mu}_{\text{eff}}$  are defined from the solution to so-called *local problems*. In the present study, we assume that all materials share the same magnetic permeability  $\mu_0$ . Hence,

$\boldsymbol{\mu}_{\text{eff}} = \mu_0 \mathbf{I}$ , and only one (complex) local problem must be solved: find  $\phi$  defined over the RVE, such that

$$\mathbf{div J} = 0, \quad (\text{B.6})$$

$$\mathbf{J} = (j\omega\epsilon + \sigma)\mathbf{E}, \quad (\text{B.7})$$

$$\mathbf{E} = \bar{\mathbf{E}} + \mathbf{grad} \phi, \quad (\text{B.8})$$

where  $\bar{\mathbf{E}}$  is the macroscopic electric field. It is prescribed by means of appropriate boundary conditions on the RVE which insure that

$$\langle \mathbf{J} \cdot \mathbf{E} \rangle = \langle \mathbf{J} \rangle \cdot \langle \mathbf{E} \rangle = \langle \mathbf{J} \rangle \cdot \bar{\mathbf{E}}, \quad (\text{B.9})$$

where  $\langle \bullet \rangle$  refers in this section to the volume average over the RVE. With such boundary conditions, this problem is well-posed (up to a constant) and the unique solution  $\phi$  depends linearly on  $\bar{\mathbf{E}}$ : there is a unique second-rank tensor  $\mathbf{X}$  such that  $\mathbf{E} = \mathbf{X} \cdot \bar{\mathbf{E}}$ . The homogenized parameters are then defined as follows

$$\epsilon_{\text{eff}} = \langle \epsilon \mathbf{X} \rangle \quad \text{and} \quad \sigma_{\text{eff}} = \langle \sigma \mathbf{X} \rangle. \quad (\text{B.10})$$

The homogenized material is isotropic if both tensors are diagonal:  $\epsilon_{\text{eff}} = \epsilon_{\text{eff}} \mathbf{I}$  and  $\sigma_{\text{eff}} = \sigma_{\text{eff}} \mathbf{I}$ .

## References

- Artola, M., Cessenat, M., 1990. Un problème raide avec homogénéisation en électromagnétisme. C. R. Acad. Sci. Paris 310, 9–14.
- Bourdi, T., Rhazi, J.E., Boone, F., Ballivy, G., 2012. Modelling dielectric-constant values of concrete: An aid to shielding effectiveness prediction and ground-penetrating radar wave technique interpretation. Journal of Physics D: Applied Physics 45, 405401. doi:10.1088/0022-3727/45/40/405401.
- Bruggeman, D.A.G., 1935. Berechnung verschiedener physikalischer Konstanten von heterogenen Substanzen. I. Dielektrizitätskonstanten und Leitfähigkeiten der Mischkörper aus isotropen Substanzen. Annalen der Physik 416, 636–664. doi:10.1002/andp.19354160705.
- Canot, H., Frénod, E., 2017. Method of Homogenization for the Study of the Propagation of Electromagnetic Waves in a Composite Part 2: Homogenization, in: Ao, S.I., Gelman, L., Hukins, D.W., Hunter, A., Korsunsky, A.M. (Eds.), Proceedings of the World Congress on Engineering 2017, Newswood Limited, London, United Kingdom. pp. 11–15.
- Cao, J., Chung, D., 2003. Colloidal graphite as an admixture in cement and as a coating on cement for electromagnetic interference shielding. Cement and Concrete Research 33, 1737–1740. doi:10.1016/S0008-8846(03)00152-2.
- Caron-Fellens, J.P., Mardiguian, M., 2017. The intelligent concrete: A new, economical technique for architectural shielding of buildings. IEEE Electromagnetic Compatibility Magazine 6, 50–54. doi:10.1109/MEMC.0.7989998.
- Chung, D., 2001. Comparison of submicron-diameter carbon filaments and conventional carbon fibers as fillers in composite materials. Carbon 39, 1119–1125. doi:10.1016/S0008-6223(00)00314-6.

- Chung, D.D.L., 2000. Cement reinforced with short carbon fibers: A multifunctional material. *Composites* doi:[10.1016/S1359-8368\(99\)00071-2](https://doi.org/10.1016/S1359-8368(99)00071-2).
- Eshelby, J.D., 1957. The determination of the elastic field of an ellipsoidal inclusion, and related problems. *The Royal Society London* 241, 376–396.
- Guan, H., Liu, S., Duan, Y., Cheng, J., 2006. Cement based electromagnetic shielding and absorbing building materials. *Cement and Concrete Composites* 28, 468–474. doi:[10.1016/j.cemconcomp.2005.12.004](https://doi.org/10.1016/j.cemconcomp.2005.12.004).
- Guihard, V., 2018. Homogénéisation de Grandeurs Électromagnétiques Dans Les Milieux Cimentaires Pour Le Calcul de Teneur En Eau. Ph.D. thesis. Paul Sabatier - Toulouse III.
- Jung, M., Lee, Y.s., Hong, S.G., Moon, J., 2020. Carbon nanotubes (CNTs) in ultra-high performance concrete (UHPC). Dispersion, mechanical properties, and electromagnetic interference (EMI) shielding effectiveness (SE). *Cement and Concrete Research* 131.
- Khadra, M., Rougelot, T., Carlier, J.P., Burlion, N., 2017. Etude de la solution interstitielle des pâtes de ciment : Extraction par injection de gaz et calcul de la conductivité électrique, in: 23e Congrès Français de Mécanique, Association Française de Mécanique, Lille.
- Krause, A., Nguyen, L., Tuan, C., Bonsell, J., Chen, B., Blasey, J.D., Zemotel, J.P., McNerney, H., Metzger, F.J., 2012. Conductive concrete as an electromagnetic shield, in: 2012 IEEE International Symposium on Electromagnetic Compatibility, IEEE, Pittsburgh, PA, USA. pp. 85–87. doi:[10.1109/ISEMC.2012.6351806](https://doi.org/10.1109/ISEMC.2012.6351806).
- Lee, Kim, Park, 2019. The Effects of Multi-Walled Carbon Nanotubes and Steel Fibers on the AC Impedance and Electromagnetic Shielding Effectiveness of High-Performance, Fiber-Reinforced Cementitious Composites. *Materials* 12, 3591. doi:[10.3390/ma12213591](https://doi.org/10.3390/ma12213591).
- Lee, J.H., Choi, J.S., Yuan, T.F., Yoon, Y.S., 2021. Shielding Effectiveness and Impact Resistance of Concrete Walls Strengthened by High-Strength High-Ductility Concrete. *Materials* 14, 7773. doi:[10.3390/ma14247773](https://doi.org/10.3390/ma14247773).
- Maxwell Garnett, J.C., 1904. Colours in metal glasses and in metallic films. *Philosophical Transactions of the Royal Society A* 203, 385–420. doi:[10.1098/rsta.1904.0024](https://doi.org/10.1098/rsta.1904.0024).
- Mazzoli, A., Corinaldesi, V., Donnini, J., Di Perna, C., Micheli, D., Vricella, A., Pastore, R., Bastianelli, L., Moglie, F., Mariani Primiani, V., 2018. Effect of graphene oxide and metallic fibers on the electromagnetic shielding effect of engineered cementitious composites. *Journal of Building Engineering* 18, 33–39. doi:[10.1016/j.jobbe.2018.02.019](https://doi.org/10.1016/j.jobbe.2018.02.019).
- Medeiros-Junior, R.A., Lima, M.G., 2016. Electrical resistivity of unsaturated concrete using different types of cement. *Construction and Building Materials* 107, 11–16. doi:[10.1016/j.conbuildmat.2015.12.168](https://doi.org/10.1016/j.conbuildmat.2015.12.168).
- Nguyen, L., Krause, A., Tuan, C., Blasey, J.D., Zemotel, J.P., McNerney, H., Metzger, F.J., 2017. Shielding effectiveness performance of conductive concrete structures, in: 2017 IEEE International Symposium on Electromagnetic Compatibility & Signal/Power Integrity (EMCSI), IEEE, Washington, DC, USA. pp. 360–363. doi:[10.1109/ISEMC.2017.8077895](https://doi.org/10.1109/ISEMC.2017.8077895).
- Ogunsola, A., Reggiani, U., Sandrolini, L., 2006. Modelling shielding properties of concrete, in: 2006 17th International Zurich Symposium on Electromagnetic Compatibility, IEEE, Singapore. pp. 34–37. doi:[10.1109/EMCZUR.2006.214862](https://doi.org/10.1109/EMCZUR.2006.214862).
- Ott, H.W., 1988. *Noise Reduction Techniques in Electronic Systems*. John Wiley and Sons, Inc.
- Paul, C.R., 2006. *Introduction to Electromagnetic Compatibility*. John Wiley and Sons, Inc.
- Quintana, S., de Blas, J.M., Peña, J., Blanco, J., García, L.D., Pastor, J.M., 2018. Design and Operation of a Real-Scale Electromagnetic Shielding Evaluation System for Reinforced Composite Construction Materials. *Journal of Materials in Civil Engineering* 30, 04018162. doi:[10.1061/\(ASCE\)MT.1943-5533.0002323](https://doi.org/10.1061/(ASCE)MT.1943-5533.0002323).
- Sanchez-Palencia, E.E., 1980. Homogenization in elasticity and electromagnetism. *Non-Homogeneous Media and Vibration Theory*, 84–128.
- Sanchez-Palencia, E.E., Sanchez-Hubert, J., 1978. Sur certains problèmes physiques d'homogénéisation donnant lieu à des phénomènes de relaxation. *C. R. Acad. Sci. Paris* 286, 903–905.
- Sandrolini, L., Reggiani, U., Ogunsola, A., 2007. Modelling the electrical properties of concrete for shielding effectiveness prediction. *IOP Publishing* 40, 5366–5372. doi:[10.1088/0022-3727/40/17/053](https://doi.org/10.1088/0022-3727/40/17/053).
- Sihvola, A.H., 1999. *Electromagnetic Mixing Formulas and Applications*. 47, Iet.
- Snyder, K., Feng, X., Keen, B., Mason, T., 2003. Estimating the electrical conductivity of cement paste pore solutions from OH-, K+ and Na+ concentrations. *Cement and Concrete Research* 33, 793–798. doi:[10.1016/S0008-8846\(02\)01068-2](https://doi.org/10.1016/S0008-8846(02)01068-2).
- Solgaard, A.O.S., Geiker, M., Edvardsen, C., Küter, A., 2014. Observations on the electrical resistivity of steel fibre reinforced concrete. *Materials and Structures* 47, 335–350. doi:[10.1617/s11527-013-0064-y](https://doi.org/10.1617/s11527-013-0064-y).
- Stefaniuk, D., Sobótka, M., Jarczewska, K., Logoń, D., Majcher, K., Musiał, M., Niewiadomski, P., Pakos, W., Rózański, A., Trapko, T., 2022. Microstructure properties of cementitious mortars with selected additives for electromagnetic waves absorbing applications. *Cement and Concrete Composites* 134, 104732. doi:[10.1016/j.cemconcomp.2022.104732](https://doi.org/10.1016/j.cemconcomp.2022.104732).
- Stratton, J.A., 1941. *Electromagnetic Theory*. McGraw-Hill Book Company.
- Vollpracht, A., Lothenbach, B., Snellings, R., Haufe, J., 2016. The pore solution of blended cements: A review. *Materials and Structures* 49, 3341–3367. doi:[10.1617/s11527-015-0724-1](https://doi.org/10.1617/s11527-015-0724-1).
- Wellander, N., 2001. Homogenization of the Maxwell Equations: Case I. Linear Theory. *Applications of Mathematics* 46, 29–51. doi:[10.1023/A:1013727504393](https://doi.org/10.1023/A:1013727504393).
- Wen, S., Chung, D., 2004. Electromagnetic interference shielding reaching 70 dB in steel fiber cement. *Cement and Concrete Research* 34, 329–332. doi:[10.1016/j.cemconres.2003.08.014](https://doi.org/10.1016/j.cemconres.2003.08.014).
- Yang, H.Y., Li, J., Ye, Q.Z., Zhang, X.C., 2002. Research on absorbing EMW properties of steel fiber concrete. *Journal of Functional Materials*.
- Yuan, T.F., Choi, J.S., Hong, S.H., Yoon, Y.S., 2021. Enhancing the electromagnetic shielding and impact resistance of a reinforced concrete wall for protective structures. *Cement and Concrete Composites* 122, 104148. doi:[10.1016/j.cemconcomp.2021.104148](https://doi.org/10.1016/j.cemconcomp.2021.104148).
- Yuan, T.F., Choi, J.S., Kim, Y.H., Yoon, Y.S., 2022. Influence of metallic grid and fiber reinforced concrete strengthening on the shielding and impact resistance of concrete walls. *Archives of Civil and Mechanical Engineering* 22, 109. doi:[10.1007/s43452-022-00427-3](https://doi.org/10.1007/s43452-022-00427-3).